Desalination and Water Treatment
www.deswater.com

doi:10.5004/dwt.2017.20281

69 (2017) 236–243
March

Falling film evaporation on a vertical corrugated plate conduit in MED

Jerin Robins Ebanesar, A. Mani*

Department of Mechanical Engineering, Indian Institute of Technology Madras, Chennai-600 036, India, Tel. +91 44 22574666, email: mania@iitm.ac.in (A. Mani)

Received 13 June 2016; Accepted 24 October 2016

ABSTRACT

Falling film evaporators are widely used in desalination, refrigeration, petroleum refining, chemical industries, etc. In falling film evaporators used in multi-effect distillation system, the latent heat released by the condensing steam is transferred to the liquid falling over the tubes which results in convective evaporation. This paper presents a two dimensional CFD study of falling film evaporation on a vertical corrugated conduit for low temperature multi-effect distillation (LT-MED) application. Two-phase flow simulation is carried out by using finite volume method based FLUENT 14.0 with turbulence model of *k*-ω equations with shear stress transport (SST). Sinusoidal corrugation with three different dimensions is selected for the study. Evaporation and heat transfer during falling film evaporation are included through user defined functions (UDFs). Present numerical results are compared with the results of horizontal tube falling film evaporation from the literature. An enhancement of 50% in film heat transfer coefficient is observed. Effects of Reynolds number and number of corrugations on heat transfer coefficient are presented.

Keywords: Falling film evaporation; MED; Vertical corrugated plate; Numerical simulation; Heat transfer enhancement

1. Introduction

Many countries in the world suffer from a shortage of portable water. Due to the rise in population rates and enhanced living standards, the need of portable water is increasing at higher rates. So, some countries depend on desalination technologies for making distilled water to meet their requirements. Multi-effect distillation (MED) is one of the oldest desalination methods and is efficient thermodynamically. Horizontal falling film evaporators are widely used in the MED plants and also in the refrigeration industries. Horizontal shell-side falling film evaporators have a significant potential to replace flooded evaporators. Compared to flooded type evaporators, falling film evaporators need less working fluid. Higher heat transfer coefficient will make the falling film evaporators dominate over the conventional flooded type evaporators. But due to shell and tube configuration, the falling film evaporators are bulky like flooded tube evaporators. Another main problem concerning about the film evaporation over horizontal tubes are the formation of dry patches. Dry patches causes reduction in heat transfer and sometimes the failure of the tubes also occurs. On the other hand vertical plate falling film evaporators are more compact, cheaper, lower fouling resistance and higher heat transfer coefficient than that of the shell and tube configuration [1–3].

Tube geometry and tube size have an important role on the performance of the falling film evaporators. Geometry of the tube can be varied by enhancing techniques and also by changing the shape of the tube. Enhancing the tube can provide better heat transfer coefficient mainly because of increase in the number of nucleation sites, increase in the total surface area and the presence of turbulence [4,5]. Luo et al. [6] reported a better heat transfer performance by using non circular tubes like oval shaped and drop shaped

*Corresponding author.

Presented at the EDS conference on Desalination for the Environment: Clean Water and Energy, Rome, Italy, 22–26 May 2016.

tubes and also they reported a lower dimensionless temperature and a thinner thermal boundary layer.

Corrugated vertical plate evaporators are developing technology in the vertical plate evaporators category. Most of the published falling film studies concern laminar and turbulent fluid flow over a horizontal tube or over a flat vertical plate compared to corrugated vertical plate. Gonda et al. [7] conducted an experimental study on falling film evaporation over a corrugated vertical plate. Around 50% increase in Nusselts number is obtained compared to smooth tube. And also Gonda et al. [7] reported that the flow regime is turbulent due to corrugated structure of the plate. The previous work which is somewhat related to vertical corrugated plate is by Kafi et al. [2]. Their studies are based on the evaporation of saline water over vertical smooth plate with horizontal metallic wires embedded on it. They reported high wetting, stability and turbulent falling film due to metallic wires on the plates.

In the present study, a numerical model is developed for falling film evaporation over corrugated conduit. Fresh water and sea water is taken for the study. A comparative study has been carried out between corrugated conduit and the circular tube.

2. Computational methods

2.1. Physical and computational domain

Fig. 1(a) shows the physical structure of horizontal falling film evaporator using corrugated conduit. From literature the present geometry is made from two stainless steel flat plates, which are welded together by horizontal lines. L is the major axis length and A is the amplitude of a single corrugated conduit. Three different dimensions with difference in number of corrugations and with same surface area are selected for the present study for finding the influence of number of corrugations on film heat transfer coefficient. Apart from that the dimensions which is used for the parametric study is taken from literature by Gonda et al. [7]. The length L is taken as 22.7 mm and amplitude A is taken as 5 mm. Fig. 1(b) shows the computational domain used for the present study with boundary conditions. Ansys FLUENT 14.0, a finite volume method based software, is used to carry out the heat transfer studies on falling film evaporation on corrugated plate. ICEM CFD is used for geometry making and meshing.

2.2. Governing equations and Boundary conditions

Pressure based solver is employed in the present model. For turbulence modeling, *k*-ω turbulence model with shear stress transport (SST) is used. The main reason is that it is a hybrid model combining the Wilcox *k*-ω and the *k*-ε models. *k*-ω is well suited for simulations inside the viscous sublayer and *k*-ε turbulence model is well suited for simulations away from the wall. So this ensures that appropriate equation is used throughout the flow field. For interface tracking volume of fluid (VOF) method is used. Compressive scheme is used for the discretization of volume fraction equation. The VOF solves two sets of continuity equations for liquid and vapour phase and a single set of momentum and energy equations for combined phase of liquid and vapour.

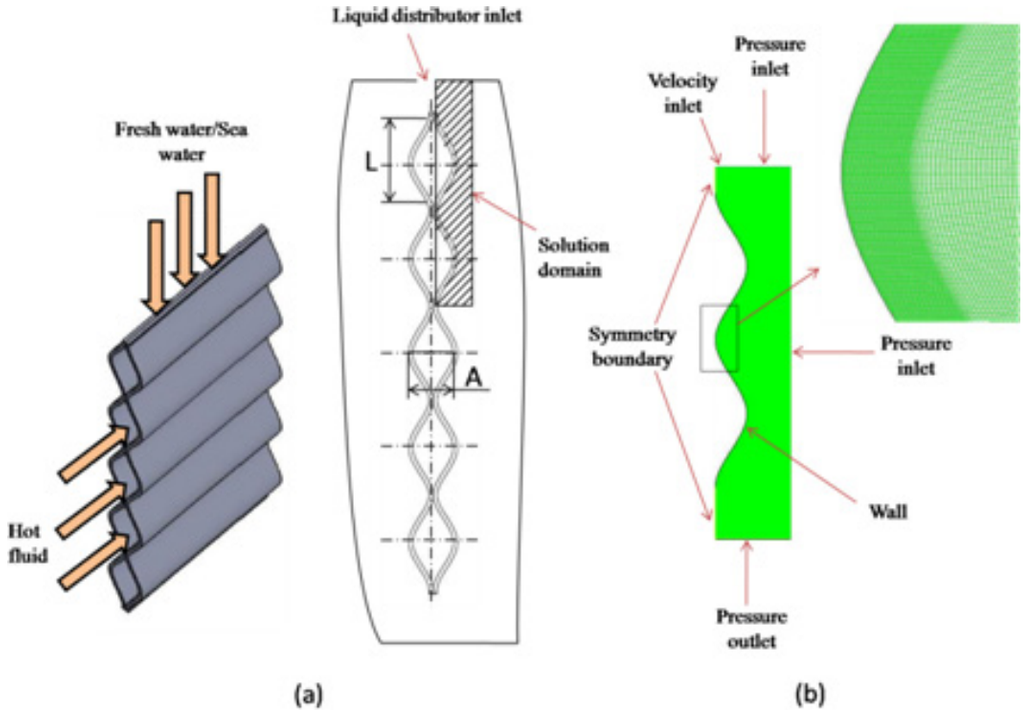

Fig. 1. (a) Physical structure of falling film evaporator and (b) Computational domain with boundary conditions.

$$\frac{\partial}{\partial t}\left(\alpha_f \rho_f\right)+\nabla\cdot\left(\alpha_f \rho_f \vec{u}_f\right)=S_f \tag{1}$$

$$\frac{\partial}{\partial t}\left(\alpha_g \rho_g\right)+\nabla\cdot\left(\alpha_g \rho_g \vec{u}_g\right)=S_g \tag{2}$$

$$\frac{\partial}{\partial t}\left(\rho\vec{u}\right)+\nabla\cdot\left(\rho\vec{u}\vec{u}\right)=-\nabla p+\nabla\cdot\left[\mu\left(\nabla\vec{u}+\nabla\vec{u}^{T}\right)\right]+\rho\vec{g}+\vec{F} \tag{3}$$

$$\frac{\partial}{\partial t}\left(\rho E\right)+\nabla\cdot\left(\vec{u}\left(\rho E+P\right)\right)=\nabla\cdot\left(k_{eff}\nabla T\right)+S_e \tag{4}$$

$$E=\frac{\alpha_f \rho_f E_f+\alpha_g \rho_g E_g}{\alpha_f \rho_f+\alpha_g \rho_g} \tag{5}$$

$$\rho=\alpha_f \rho_f+\alpha_g \rho_g \tag{6}$$

$$\mu=\alpha_f \mu_f+\alpha_g \mu_g \tag{7}$$

$$k_{eff}=\alpha_f k_f+\alpha_g k_g \tag{8}$$

The boundary conditions are as follows,
At inlet boundary condition:

$$v=v_{in},\quad u=0,\quad T=T_{sat} \tag{9}$$

$$\alpha_g=1 \quad \text{and} \quad \alpha_f=0$$

Pressure inlet boundary condition is defined as follows:

$$\frac{\partial u}{\partial y}=0,\quad \frac{\partial v}{\partial y}=0,\quad \frac{\partial T}{\partial y}=0 \tag{10}$$

$$\frac{\partial u}{\partial x}=0,\quad \frac{\partial v}{\partial x}=0,\quad \frac{\partial T}{\partial x}=0 \tag{11}$$

$$T=T_{sat},\quad \alpha_g=1 \quad \text{and} \quad \alpha_f=0$$

Pressure outlet boundary condition is defined as follows:

$$\frac{\partial u}{\partial y}=0,\quad \frac{\partial v}{\partial y}=0,\quad \frac{\partial T}{\partial y}=0 \tag{12}$$

$$T=T_{sat},\quad \alpha_g=1 \quad \text{and} \quad \alpha_f=0$$

Symmetry boundary condition is as follows:

$$\frac{\partial u}{\partial x}=0,\quad \frac{\partial v}{\partial x}=0,\quad \frac{\partial T}{\partial x}=0 \tag{13}$$

At Wall boundary:

$$T=T_w \tag{14}$$

2.3. Phase Change Model

Main challenge of simulation of two-phase flow is considering the heat and mass transfer during phase change. Several phase change models are proposed in literature. The commonly used phase change model for evaporation and condensation is proposed by Lee [8], which is derived from Hertz–Knudsen (15) and Clausius–Clapeyron (16) equations. Eq. (17) gives the mass source term from Lee model. The main drawback of Lee model, which is reported by Kharangate et al. [9], is that the evaporation will occur at everywhere as long as $T \geq T_{sat}$ condition is satisfied. That is, evaporation source term is applied not only at the interface, but also in the liquid phase when the above condition is satisfied. Physically this is not possible during any convective evaporation process, where evaporation occur only at the interface.

$$J'=\alpha_c\frac{\sqrt{M}}{2\pi R}\left(\frac{p}{\sqrt{T_g}}-\frac{p_{sat}\left(T_f\right)}{\sqrt{T_f}}\right) \tag{15}$$

$$\frac{dp}{dT}=\frac{\Delta H}{T\left(\frac{1}{\rho_f}-\frac{1}{\rho_g}\right)} \tag{16}$$

$$S_g=-S_f=r_i\alpha_f\rho_f\frac{\left(T-T_{sat}\right)}{T_{sat}} \tag{17}$$

$$T\geq T_{sat}$$

Another phase change model is proposed by Tanasawa, which is also derived from Hertz–Knudsen (15) equation. Eqs. (18) and (19) give the mass flux and mass source term respectively from Tanasawa model.

$$\dot{m}''=\frac{2\gamma}{2-\gamma}\sqrt{\frac{M}{2\pi R}}\frac{\rho_g h_{fg}\left(T-T_{sat}\right)}{T_{sat}^{3/2}} \tag{18}$$

$$S_g=-S_f=\dot{m}''\left|\nabla\alpha_g\right| \tag{19}$$

From literatures [9–12] reported that interfacial temperature obtained by means of Lee and Tanasawa numerical technique will not be exactly the saturation temperature. The empirical constants r_i used in Lee model and the constant γ used in Tanasawa model does not have any physical limits. Therefore, excessively small values of these empirical constants lead to a significant deviation between interfacial and saturation temperature. However, too large values cause convergence problems and therefore optimal values must be found for r_i and γ.

Third phase change model, which is used in the present study, is called sharp interface model, which uses the Rankine–Hugoniot jump condition for energy conservation at the interface. This model is purely theoretical and does not depend upon any empirical constants. The interfacial heat flux jump and mass flux can be calculated by the following Eqs. (20) and (21) respectively.

$$q_i''=-k_{eff}\left(\nabla T_i\cdot\vec{n}\right) \tag{20}$$

$$\dot{m}'' = \frac{-k_{eff}\left(\nabla T_i \cdot \vec{n}\right)}{h_{fg}} \tag{21}$$

Mass and energy source terms calculated from sharp interface model is given in Eqs. (22) and (23) respectively.

$$S_g = -S_f = \dot{m}''\left|\nabla \alpha_g\right| = \frac{k_{eff}\left(\nabla \alpha_g \cdot \nabla T\right)}{h_{fg}} \tag{22}$$

$$S_e = S_f h_{fg} \tag{23}$$

2.4. Grid and Time Step Size

Three geometries with difference in number of corrugations are selected for the present study. All three geometries have same surface area. Mesh independence studies are carried out for all geometries. Boundary layer meshing method is used and y^+ value of less than 5 is taken for the calculation of first layer thickness. Structured mesh is used for the entire domain. The convergence criteria used for the present model is 10^{-6} for energy equation and 10^{-4} for both continuity and momentum equation. Time independent study also carried out. The time step used for the present study is 10^{-4} s for all three geometries.

3. Results and discussion

3.1. Heat transfer coefficient

Operational parameters of heat transfer studies are given in the Table 1. Both fresh water and sea water is taken for the studies. At Reynolds numbers as low as 400, film breakdown occurred and because of that getting a converged solution was difficult. So the present simulations are done for Reynolds number higher than 550. For the calculation of film evaporative heat transfer coefficient, value of wall heat flux is calculated, at various locations, after a steady film is formed and Eq. (24) is used to calculate the local film heat transfer coefficient. Eqs. (25) and (26) give the average film heat transfer coefficient and average Nusselt number respectively.

Table 1
Specification of operating conditions for the present study

Case	1	2	3
Working fluid	Fresh water	Fresh water	Seawater
Inlet Reynolds number (Re) range	275–6746	1180–1940	952–2182
Inlet temperature range (°C)	10–60	60	60–70
Wall super heat (°C)	3	3	3
Number of corrugations	2	2, 3, 4	2
Prandtl number (Pr) range	9.44–2.983	2.983	2.7–2.983

$$h = \frac{q_w}{T_w - T_{sat}} = \frac{-k_f \left.\frac{\partial T}{\partial y}\right|_{y=0}}{T_w - T_{sat}} \tag{24}$$

$$\bar{h} = \frac{1}{2\pi}\int_0^{2\pi} h\, d\phi \tag{25}$$

$$\overline{N_u} = \frac{\bar{h}}{k_f}\left[\frac{\mu_f^2}{\rho_f^2 g}\right]^{1/3} \tag{26}$$

In order to validate the present numerical solution an experimental study by Gonda et al. [7] from literature is selected and the validation is shown in Fig. 2. Geometry shape, dimensions and the operating conditions except the heating method are same as that of the experimental studies. It can be seen that, at higher Reynolds number, the current numerical results are in good agreement with the deviation of less than 13%. But at lower Reynolds numbers, the prediction by the present numerical model is poor. It is mainly because of the assumption made, the flow become turbulent at lower Reynolds numbers.

Fig. 3 shows the comparison between the present numerical study about film evaporation over the corrugated conduit and smooth tube from literature. Details about the literature studies are listed in the Table 2. About 50% enhancement in heat transfer is observed by comparing the present results with results of Han and Fletcher [13]. The heat transfer rate is higher for corrugated conduit compared to circular tube. It is mainly due to the following reasons. Firstly, the effective contact area between the corrugated conduit and the liquid film is larger. Secondly, the liquid film is turbulent because of the sinusoidal shape of the corrugated conduit which will increase the heat transfer coefficient of the falling film. Both contact area and the heat transfer coefficient are directly proportional to heat transfer rate according to the Eq. (27).

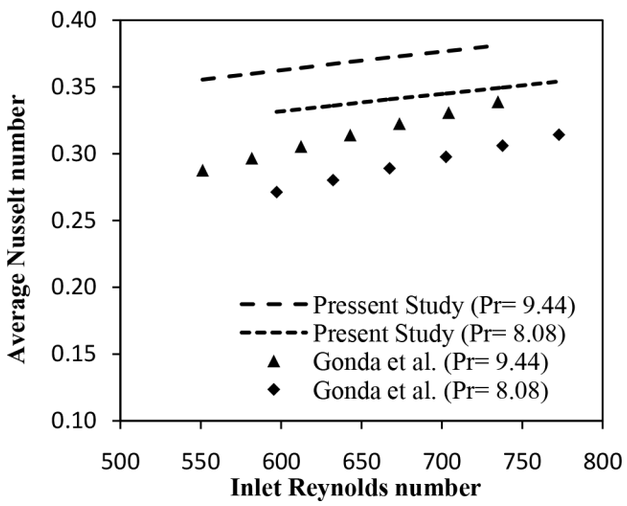

Fig. 2. Comparison of present study with the literature on experimental study.

$$\dot{Q} = \overline{h} A_C \Delta T \quad (27)$$

Fig. 4 shows the comparison between sea water and fresh water in order to demonstrate the difference in heat transfer characteristics. Sea water with salinity of 35 g/kg is used for the study and the properties of sea water is selected from the literature [15] and are included in the solver through UDFs. Studies by Mu et al. [16] reported that heat transfer coefficient is less for sea water films. For the present study average Nusselt number is analysed and it is higher for sea water compared to fresh water but taking heat transfer coefficient in to account, fresh water possess higher heat transfer coefficient which backs the literature [16]. Film coefficient is low for sea water mainly due to the high viscosity and surface tension effects. Fig. 5 shows the variation of average Nusselt number with inlet Reynolds number for different Prandtl numbers. Nusselt number is higher at higher Reynolds numbers and higher Prandtl numbers.

Three geometries with same surface area and different number of corrugations are shown in Fig. 6 are selected for the study and all dimensions indicated in the figure

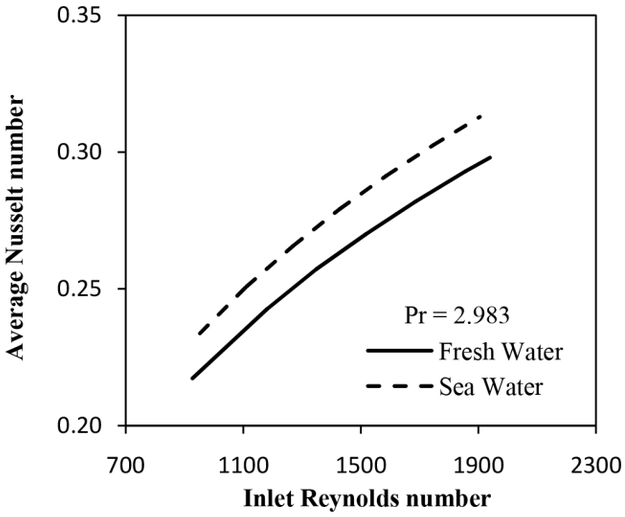

Fig. 4. Comparison on average Nusselt number between sea water and fresh water.

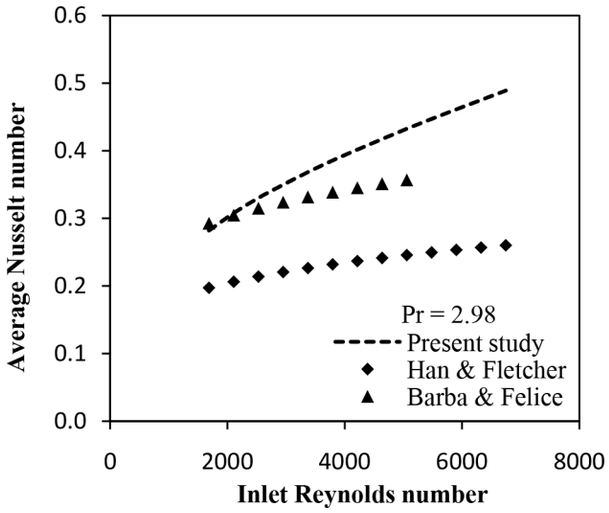

Fig. 3. Comparison of present study results with horizontal smooth circular tube from literature.

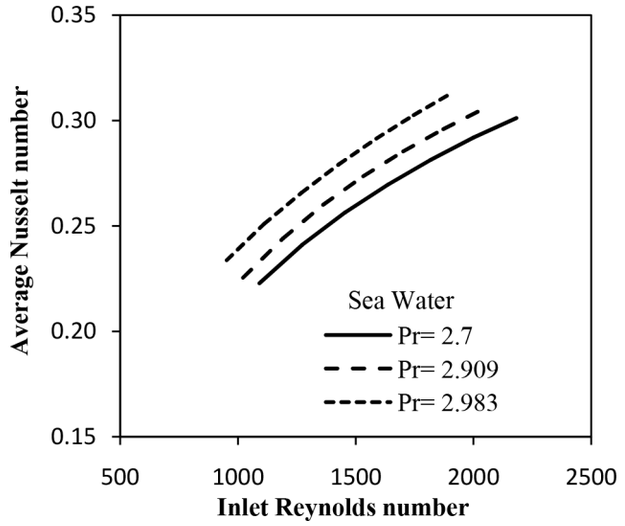

Fig. 5. Variation of average Nusselt number with inlet Reynolds number.

Table 2
Some studies on falling film evaporation from literature

Authors	Study in Brief	*Pr* range	*Re* range	Correlations for film heat transfer coefficient
Gonda et al. [7]	Water film evaporation over corrugated conduit. 26 corrugated channels having an external area of 0.267 m^2.	7.4–10.45	230–790	$Nu = 0.00175\, Re^{0.57}\, Pr^{0.67}$
Han and Fletcher [13]	Water falling film evaporation over horizontal smooth, circumferentially grooved and axially grooved 50.8 mm diameter brass tubes of length 254 mm.	1.3–3.6	770–7000	$Nu_{tur} = 0.025\, Re^{0.2}\, Pr^{0.53}$ (smooth tube)
Barba and Felice [14]	Theoretical approach for the prediction of evaporation heat transfer coefficient in a horizontal falling film.	1–5	1500–5000	$\overline{h}\left(\frac{\mu^2}{g\rho^2 k^3}\right)^{1/3}_{tur} = 0.046 Re^{0.18} Pr^{0.47}$

are in mm. Fig. 7 shows the variation of average Nusselt number with Reynolds number and for different corrugations. Fresh water is used for the study. From the results, it is found that number of corrugations have a small impact on average Nusselt number. Maximum increment of only 3% is observed by comparing the 2 number of corrugations with 3 and 4 number of corrugations. And also, not much variations in Nusselt number is observed by comparing the results of corrugation number 3 and 4. As mentioned earlier, with same surface area, there is only one possibility for getting higher heat transfer is by increase in turbulence. So the reason may be for not getting higher heat transfer is because of lack of increase in turbulence effects with increase in corrugation.

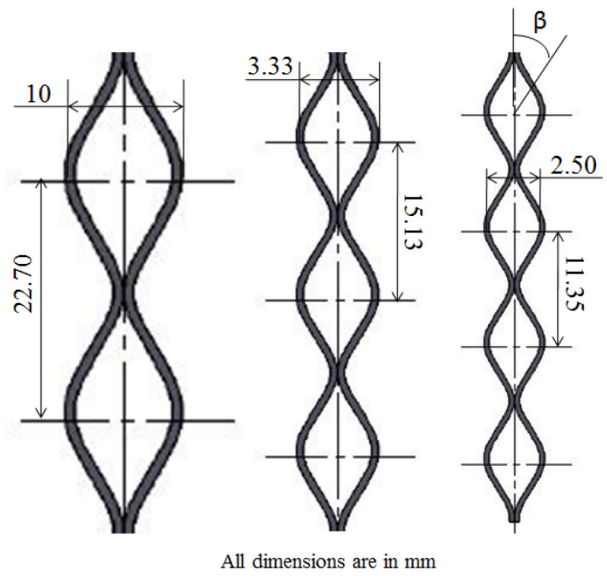

Fig. 6. Geometries with 2, 3 and 4 number of corrugations.

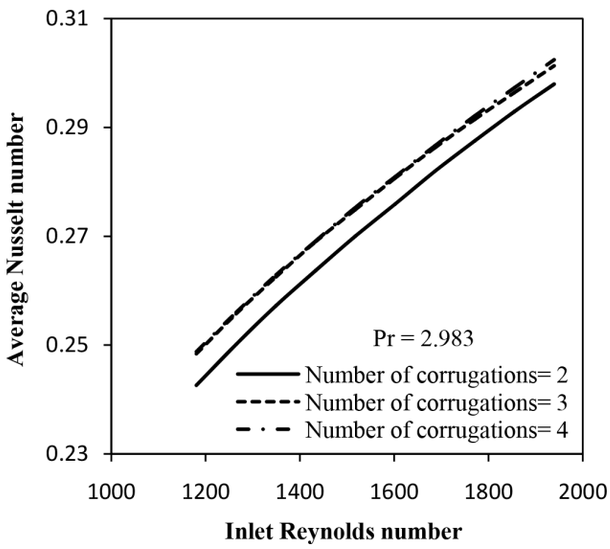

Fig. 7. Variation of heat transfer coefficient for different corrugations.

3.2. Film Thickness

Fig. 8 illustrates the variation of the liquid film thickness as a function of angular position; β of a single corrugation. The observed trend of film thickness distribution is not matching with the Nusselt model, which is based on laminar flow assumption whereas present simulation is based on the turbulent flow assumption.

Variation of film thickness distribution of water with different Reynolds number is shown in the Fig. 9, which shows that the film thickness increases with increase in flow rate. Unlike horizontal tubes, film thickness is almost same as the flow reaches downstream. For horizontal tubes, maximum film thickness is observed at top and bottom of the tube.

Fig. 10 shows the variation of gravity component tangent to the wall (G_T) with curve length of both corrugated surface and circular surface. The corrugated surface is

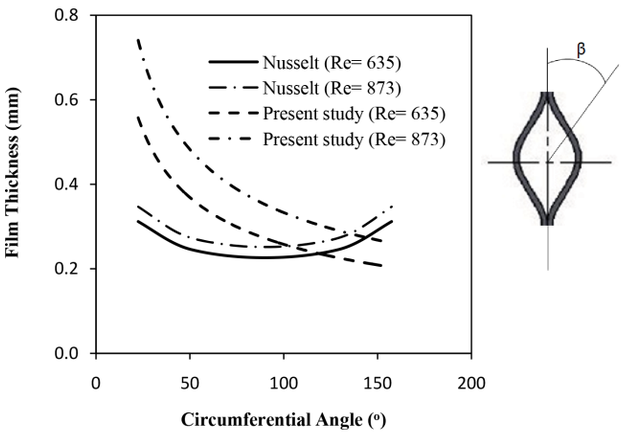

Fig. 8. Comparison of film thickness along the surface of a single corrugation.

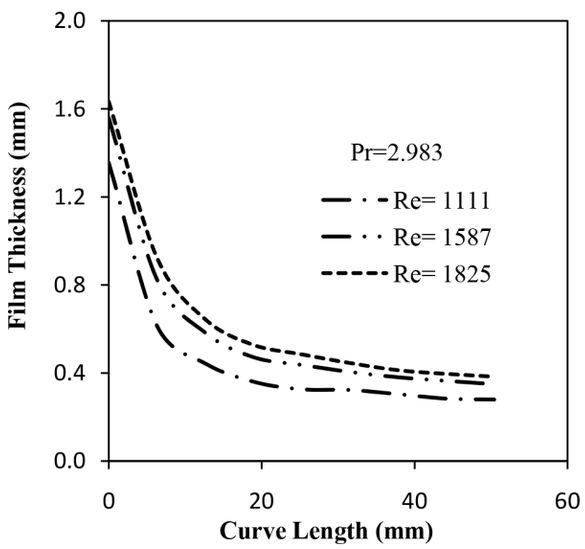

Fig. 9. Variation of film thickness along the perimeter for different *Re*.

assumed to be sinusoidal. The tangential component of gravity for corrugated and circular surface is given in Eqs. (28) and (29) respectively.

$$G_T = \frac{g}{\sqrt{1+(2\pi A)^2 \sin^2(2\pi x)}} \tag{28}$$

$$G_T = g\sin(x) \tag{29}$$

It can be seen that the film thickness distribution is highly related to the circumferential position which directly determines the direction and value of tangential acceleration. The tangential acceleration thus varies in the same way as the tangential component force of gravity. By increasing the effect of gravity on the evaporating film, the mean film velocity at a given stream wise location is increased which results in a thinning of the evaporative film and increased heat transfer. The thickness of the film is controlled by the rate of evaporation and the film mean velocity which is dependent on gravity. Compared to circular tube, for corrugated conduit the gravity component is more dominant.

3.3. Temperature Profile

Fig. 11 shows the variation of non-dimensional temperature $\left(\theta = \frac{T - T_s}{T_w - T_s}\right)$ with non-dimensional film thickness $\left(\eta = \frac{y}{\delta}\right)$ of falling film, for different inlet Reynolds number, at a curve length of 25.2 mm. With increase in Reynolds number film temperature gradient near the heating surface increases. It is because of increase in turbulence with the flow rate.

Fig. 12 depicts the variation of non-dimensional temperature profiles across the liquid film at five different axial locations for *Re* = 1686 and *Pr* = 2.983. For the smaller curve lengths, the temperature gradient at the interface is very small. Most of the wall heat flux is used to sensible heating of the liquid film comparing to phase change. So the liquid film is thermally developing at the interface at curve lengths (*Xc*) of 6.3 mm and 12.6 mm. But for larger curve lengths 25.2 mm, 37.8 mm and 44.12 mm a steep temperature gradients can be seen at both wall and at the interface. Once the liquid film reached thermally fully developed condition, the wall heat flux is used for phase change at the interface instead of sensible heating of the liquid film.

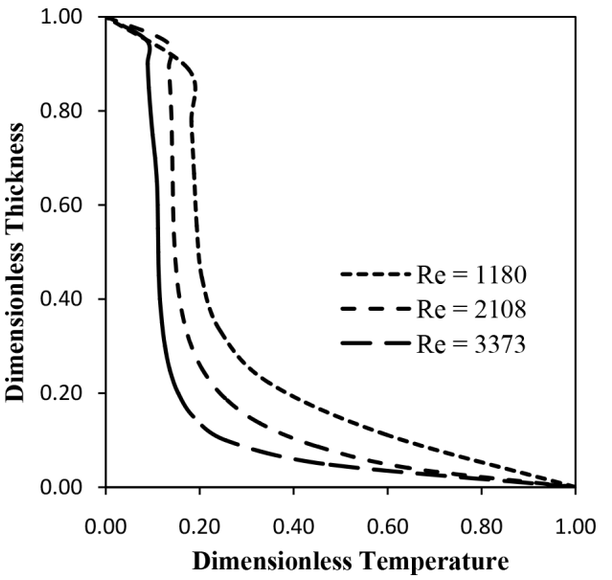

Fig. 11. Variation of non-dimensional thickness with non-dimensional temperature across the film for different Reynolds number.

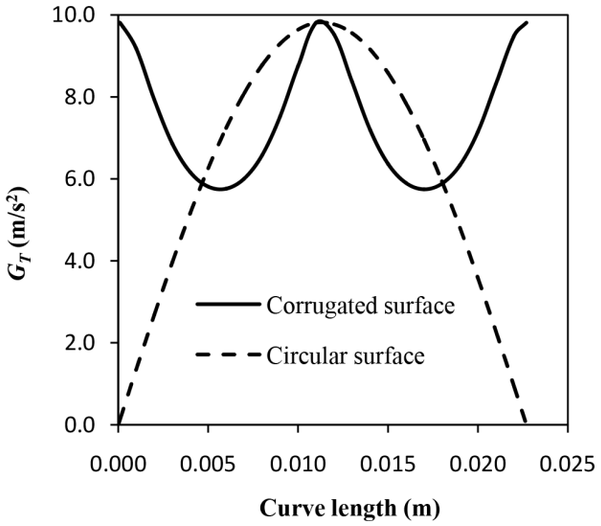

Fig. 10. Variation of tangential component of gravitational acceleration with curve length.

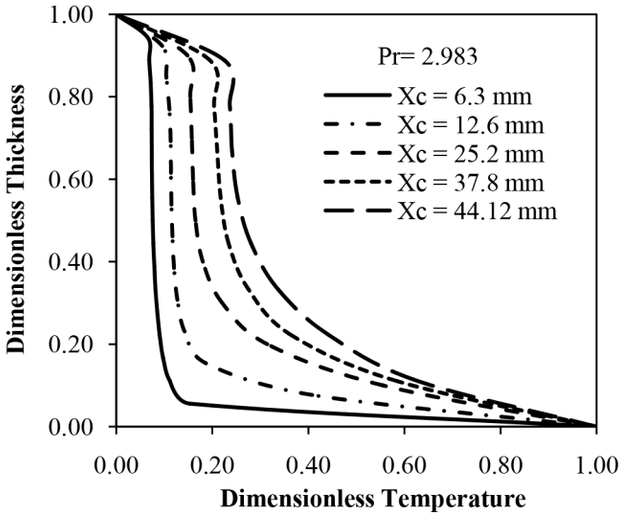

Fig. 12. Variation of dimensionless thickness with dimensionless temperature at various axial locations.

4. Conclusions

Present numerical study examined the fluid flow and heat transfer characteristics of falling film evaporation over a corrugated conduit. Based on the analysis following conclusions are drawn. The simulations are done for Reynolds numbers higher than 550.

- Unlike falling film over horizontal tube, the film thickness is mainly controlled by gravitational force in corrugated conduit. So a finite thickness is ensured over the surface and unlike horizontal tube where dry patches are seen at bottom of the tubes because of flow separation which is not observed in corrugated conduits.
- Liquid film heat transfer in the corrugated conduit is better than that of circular tube. At least 50% enhancement in heat transfer is observed.
- Heat and mass transfer across the interface is successfully captured with the aid of the sharp interface phase change model. Interfacial temperature reached saturation temperature, after reaching steady state with a maximum deviation of + 0.5°C, for every simulation.
- Three geometries with same surface area and different number of corrugations are selected for the study. It is found that number of corrugations have a small impact on heat transfer performance of a corrugated conduit.

Symbols

A_C — Contact area between liquid film and heat transfer surface
E — Energy per unit mass
g — Acceleration due to gravity
h — Heat transfer coefficient
h_{fg} — Latent heat of vaporization
k — Thermal conductivity
M — Molecular weight
N_u — Nusselt number
Pr — Prandtl number
p — Pressure
$\dot{Q}$ — Heat transfer rate
q_w — Wall heat flux
R — Universal gas constant
Re — Film Reynolds number, $\frac{4\Gamma}{\mu_f}$
r_i — Mass transfer intensity factor
S — Volumetric mass source term
T — Temperature
ΔT — Wall super heat
Y^+ — Dimensionless distance perpendicular to the wall, $\frac{yu^+}{\upsilon_f}$
Y — Distance perpendicular to the wall

Greek

ρ — Density
μ — Dynamic viscosity
Γ — Mass flow rate per unit length
θ — Dimensionless temperature
η — Dimensionless film thickness
β — Polar angle
δ — Film thickness

Subscripts

eff — Effective
e — Energy
f — Liquid
g — Vapour
sat — Saturation
tur — Turbulent
w — Wall

References

[1] R. Abraham, A. Mani, Experimental studies on thermal spray-coated horizontal tubes for falling film evaporation in multi-effect desalination system, Desal. Water Treat., 56 (2015) 71–82.
[2] F. Kafi, V. Renaudin, D. Alonso, J.M. Hornut, New med plate desalination process: thermal performances, Desalination, 166 (2004) 53–62.
[3] R. Abraham A. Mani, Heat transfer characteristics in horizontal tube bundles for falling film evaporation in multi-effect desalination system, Desalination, 375 (2015) 129–137.
[4] R. Abraham A. Mani, Effect of flame spray coating on falling film evaporation for multi-effect distillation system, Desal. Water Treat., 51 (2013) 822–829.
[5] G. Ribatski A.M. Jacobi, Falling film evaporation on horizontal tubes-a critical review, Int. J. Refrige., 28 (2005) 635–653.
[6] L.-c. Luo, G.-m. Zhang, J.-h. Pan M.-c. Tian, Flow and heat transfer characteristics of falling water film on horizontal circular and non-circular cylinders, J. Hydrodynamics, 25 (2013) 404–414.
[7] A. Gonda, P. Lancereau, P. Bandelier, L. Luo, Y. Fan, S. Benezech, Water falling film evaporation on a corrugated plate, Int. J. Thermal Sci., 81 (2014) 29–37.
[8] W.H. Lee, A pressure iteration scheme for two-phase flow modeling, in: T. N. Veziroglu (Ed.), Multiphase Transport Fundamentals, Reactor Safety, Applications, vol. 1, Hemisphere Publishing, Washington. DC, 1980.
[9] C.R. Kharangate, H. Lee, I. Mundawar, Computational modeling of turbulent evaporating falling films, Int. J. Heat Mass Transfer., 81 (2015) 52–62.
[10] R. Kouhikamal, S.M.A. Noori Rahim Abadi, M. Hassani, Numerical investigation of falling film evaporation of multi-effect desalination plant, Appl. Thermal Eng., 70 (2014) 477–485.
[11] S.C.K. De Schepper, G.J. Heynderickx, G.B. Marin, Modeling the evaporation of a hydrocarbon feedstock in the convection section of a steam cracker, Comp. Chem. Eng., 33 (2009) 122–132.
[12] D. Sun, J. Xu, Q. Chen, Modeling of the Evaporation and Condensation Phase-Change Problems with FLUENT, Numer. Heat Transfer, 66 (2014) 326–342.
[13] W.H. Parken, L.S. Fletcher, V. Sernas, J.C. Han, Heat transfer through falling film evaporation and boiling on horizontal tubes, Trans. ASME, 112 (1990) 744–750.
[14] D. Barba, R. Di Felice, Heat transfer in turbulent flow on a horizontal tube falling film evaporator, a theoretical approach, Desalination, 51 (1984) 325–333.
[15] M.H. Sharqawy, J.H. Lienhard, S.M. Zubair, Thermophysical properties of seawater: a review of existing correlations and data, Desal. Water Treat., 16 (2010) 354–380.
[16] X. Mu, S. Shen, Y. Yang, X. Liu, Experimental study of falling film evaporation heat transfer coefficient on horizontal tube, Desal. Water Treat., 50 (2012) 310–316.